Dynamics of interacting electrons under effect of a Morse potential

J. L. L. dos Santos,[1] M. O. Sales,[1] A. Ranciaro Neto,[1,2] and F. A. B. F. de Moura[1]

[1]*Instituto de Física, Universidade Federal de Alagoas, Maceió AL 57072-970, Brazil*
[2]*Faculdade de Economia, Administração e Contabilidade, Universidade Federal de Alagoas, Maceió AL 57072-970, Brazil*

We consider interacting electrons moving in a nonlinear Morse lattice. We set the initial conditions as follows: electrons were initially localized at the center of the chain and a solitonic deformation was produced by an impulse excitation on the center of the chain. By solving quantum and classical equations for this system numerically, we found that a fraction of electronic wave function was trapped by the solitonic excitation, and trapping specificities depend on the degree of interaction among electrons. Also, there is evidence that the effective electron velocity depends on Coulomb interaction and electron-phonon coupling in a nontrivial way. This association is explained in detail along this work. In addition, we briefly discuss the dependence of our results with the type of initial condition we choose for the electrons and lattice.

I. INTRODUCTION

Time evolution of interacting electrons under effect of electron-phonon coupling is an interesting theme that has direct association with electrical properties of materials. In a one electron alloy, the interaction between electrons and optical phonons can be effectively described by a nonlinear Schrödinger equation [1]. Given the background, the most interesting phenomenon related to the effective electron-electron term is called self trapping (ST). The ST transition occurs when the nonlinearity strength exceeds a critical value that has the same order of the bandwidth [2–6]. It is worth mentioning Davydov's contribution to the study of free electrons under effect of lattice vibration. He developed a model that assumed a nonlinear interaction between a linear electronic model and a linear lattice. It led to an important result: an electron-lattice nonlinear term promotes charge transport [7–11].

More recently, Velarde and coworkers demonstrated the existence of a new kind of "quasiparticle" in nonlinear lattices and they also have shown its importance to the noninteracting electron dynamics [12–27]. This new "quasi-particle" is a consequence of the coupling between self-trapped states and the lattice solitons (it was termed as *solectron*). The electronic transport mediated by lattice solitons was also investigated in several two-dimensional anharmonic lattices, particularly in a square lattice similar to the *cuprate* lattice [25]. They found numerical evidence of electron-soliton transfer along crystallographic axes. Electronic transport mediated by acoustic lattice soliton excitations was also obtained in triangular anharmonic lattices [27].

Some experimental investigations on electron dynamics under the presence of electron-lattice interaction can be found in Refs. [28–31]. For example, in Ref. [29] the authors arrested a single electron in a quantum dot and they drove it along a channel up to a another quantum dot using a surface acoustic wave (SAW). After changing SAW direction several times, the electron moved from one dot to another and back again like a ball in a table tennis game. The authors obtained up to 60 shots with good quality. In general terms, the electronic transport mediated by SAW is a direct consequence of the effective electron-lattice interaction. When a SAW propagates along an piezoelectric material such as GaAs substrate, that generates an electrostatic field. The electron is captured by this electrostatic field and propagates along the channel [29]. It was revealed the possibility of using this "controlled motion" in the framework of quantum computing. For example, a quantum "bit" can be moved between two distant places. The possibility of using SAW to move electrons and construct quantum bits has attracted immense interest [28,32–36].

The competition between the electron-lattice term and the electron-electron interaction has been the subject of recent investigations [37–41]. In Ref. [37], it was demonstrated that depending on the degree of nonlinearity and Hubbard interaction, the slope of electronic dispersion close to the Fermi level had a significant decrease. The dynamics of two correlated electrons in an anharmonic Morse-Toda lattice chain was investigated in Ref. [38]. It was demonstrated that the nonlinear coupling between the lattice vibrations and the electrons promote the transport of paired electrons [38]. In Ref. [37], the problem of two interacting electrons coupled to dispersive phonons in a nonlinear lattice was investigated. By using numerical methods, an interesting collection of discrete breathers modes induced by the electron-phonon coupling was obtained. The interplay between electron-electron and electron-phonon interactions was studied in Ref. [41]. The authors considered the time evolution of two electrons initially close to each other in a 1D crystalline nonlinear chain. It was shown that the magnitude of the electron-phonon coupling χ necessary to promote the self-trapping decreases as the electron-electron interaction U is increased [41].

Here, we consider the competition between the electron-lattice coupling and electron-electron interaction. In most of the work, we make three assumptions in addition to the basic electron-lattice model: (1) The two electrons are in the singlet subspace moving in a nonlinear Morse lattice; (2) they are initially fully localized at the center of chain; (3) the vibrational energy is introduced at the nonlinear lattice by using an impulse excitation in the same region as the initial electronic wave position. We solve the quantum and classical equations for this problem and we track the electronic dynamics. Our results suggest that both electrons are trapped by the solitonic

excitation. The numerical calculation also shows nontrivial dependence of the effective electron velocity on the Coulomb interaction and on electron-lattice coupling. We also discuss electron wave-function trapping in the view of the bound electronic states. We briefly examine the dependence of our results with the type of initial conditions we choose for the electrons and lattice.

II. MODEL AND NUMERICAL CALCULATION

We consider two-electrons moving in a 1D anharmonic lattice of N masses. The complete Hamiltonian for the electron and lattice can be written as $H = H_{\text{lattice}} + H_{\text{ele}}$. Here, H_{ele} is a two-electron Hamiltonian defined as [38,42]

$$H_{\text{ele}} = -\sum_{n,\sigma}(T_{n,n-1}a_{n,s}^{\dagger}a_{n-1,s} + T_{n,n+1}a_{n,s}^{\dagger}a_{n+1,s})$$
$$+ U\sum_{n}a_{n,\uparrow}^{\dagger}a_{n,\uparrow}a_{n,\downarrow}^{\dagger}a_{n,\downarrow}. \quad (1)$$

$a_{n,s}^{\dagger}$ and $a_{n,s}$ are the creation and annihilation operators for the electron with spin s at site n. $T_{n,n+1}$ is the hopping amplitude between sites n and $n+1$. U represents the electron-electron interaction (the Coulomb interaction) [43]. H_{lattice} represents the classical Hamiltonian of N masses coupled by the Morse potential,

$$H_{\text{lattice}} = \sum_{n}\left(\frac{p_n^2}{2M_n} + D\{1 - e^{[-B(q_n-q_{n-1})]}\}^2\right), \quad (2)$$

where p_n and q_n are the momentum and displacement of the mass at site n, respectively. For the sake of simplicity, we take all particles with identical masses ($M_n = 1$). We also use the dimensionless representation by absorbing the constants D and B as follows [16]: $q_n \rightarrow Bq_n$, $p_n \rightarrow p_n/\sqrt{2D}$, and $H_{\text{lattice}} \rightarrow H_{\text{lattice}}/(2D)$. The coupling between these two Hamiltonians is introduced by considering the electronic hopping $T_{n,n+1}$ as a function of the displacement $q_{n+1} - q_n$. Following Ref. [16], we get $T_{n,n+1} = -T_0\exp[-\alpha(q_{n+1} - q_n)]$. The quantity α represents electron-lattice interaction degree (in units of $1/B$). For small relative displacement we recover the Su-Schrieffer-Heeger approximation $T_{n,n+1} \approx -T_0[1 - \alpha(q_{n+1} - q_n)]$ [44].

The time-dependent two-electron wave function is obtained by numerical solution of the time-dependent Schrödinger equation. By using the Wannier representation, the two-particles wave packet may be written as $|\Psi(t)\rangle = \sum_{n,m}c_{n,m}(t)|n,m\rangle$. Here, the *ket* $|n,m\rangle$ represents a state with one electron with spin $\uparrow$ at site n and the other electron with spin $\downarrow$ at site m. Wannier amplitudes ($c_{n,m}(t)$) evolve in time according to the time-dependent Schrödinger equation as ($\hbar = 1$)

$$i\hbar\frac{dc_{n,m}}{dt} = -\tau\{e^{[-\alpha(q_m-q_{m-1})]}c_{n,m-1}$$
$$+ e^{[-\alpha(q_{m+1}-q_m)]}c_{n,m+1}$$
$$+ e^{[-\alpha(q_n-q_{n-1})]}c_{n-1,m}$$
$$+ e^{[-\alpha(q_{n+1}-q_n)]}c_{n+1,m}\} + Uc_{n,m}\delta_{n,m}. \quad (3)$$

Lattice equation is written as

$$\frac{d^2q_n}{dt^2} = \{1 - e^{[-(q_{n+1}-q_n)]}\}e^{[-(q_{n+1}-q_n)]}$$
$$- \{1 - e^{[-(q_n-q_{n-1})]}\}e^{[-(q_n-q_{n-1})]}$$
$$+ \alpha T_0 e^{[-\alpha(q_{n+1}-q_n)]}\sum_m\{[c_{m,n+1}^*c_{m,n} + c_{m,n}^*c_{m,n+1}]$$
$$+ [c_{n+1,m}^*c_{n,m} + c_{n,m}^*c_{n+1,m}]\}$$
$$- \alpha T_0 e^{[-\alpha(q_n-q_{n-1})]}\sum_m\{[c_{m,n}^*c_{m,n-1} + c_{m,n-1}^*c_{m,n}]$$
$$+ [c_{n-1,m}^*c_{n,m} + c_{n,m}^*c_{n-1,m}]\}. \quad (4)$$

We notice that right side of the quantum equation [Eq. (3)] was multiplied by the quantity τ. Here $\tau = T_0/(\hbar\Omega)$ where Ω is the frequency of harmonic oscillations around the minimum of the Morse potential. The generalized hopping τ determines the time scale difference between the fast electronic dynamics and the slow lattice vibrations.

Our calculations are made using precise numerical solution of the previous Eqs. (3) and (4). The equations of electron motion [Eq. (3)] are solved numerically employing a high-order method based on the Taylor expansion of time evolution operator $\tilde{O}(\delta t) = e^{(-i\tilde{H}_{\text{ele}}\delta t)} = 1 + \sum_{l=1}^{n_o}(-i\tilde{H}_{\text{ele}}\delta t)^l)/(l!)$ [42,45,46]. Here, $\tilde{H}_{\text{ele}}$ is exactly the same one electron Hamiltonian [Eq. (1)] with normalized hopping $\tilde{T}_{n,n+1} = -\tau\exp[-\alpha(q_{n+1} - q_n)]$. The wave-function at time δt is given by $|\Psi(\delta t)\rangle = \tilde{O}(\delta t)|\Psi(t = 0)\rangle$. This method can be used recursively to get the wave-function at time t.

The classical equations [Eq. (4)] are solved by using a predictor-corrector Euler method defined as following [47,48]: The procedure starts by adopting a standard Euler method in order to find a prediction $q_n(\delta t)^* \approx q_n(t = 0) + \delta t[(dq_n/dt)|_{t=0}]$ at time δt. The next step consists of applying a correction formula in order to get the approximation improved, i.e., $q_n(\delta t) \approx q_n(t = 0) + (\delta t/2)[(dq_n/dt)|_{t=0} + (dq_n^*/dt)|_{\delta t}]$. In our computation, this formula is recursively applied three times.

The sum of the evolution operator was truncated at $n_o = 12$ and $\delta t = 10^{-2}$. By using this Taylor-Euler formalism we could keep the wave-function norm within the following numerical tolerance: $|1 - \sum_{n,m}|c_{n,m}(t)|^2| < 10^{-8}$ along the entire time interval. The calculation of norm conservation is a first and important check for the accuracy of our numerical procedure. Besides, in order to provide a second check, we also solve Eqs. (3) and (4) by using standard fourth-order Runge-Kutta (RK4) [47]. The results obtained by both methods (Taylor-Euler and RK4) do not show any qualitative difference. However, the Taylor-Euler method requires lees time than standard (RK4) formalism to achieve same dynamics (on average, time ratio is approximately one-third).

In order to understand the two-electron dynamics on this nonlinear model, we computed the wave-packet centroid of each electron defined as [48,49]

$$\langle m\rangle(t) = \sum_{n,m}[m]|c_{n,m}(t)|^2, \quad (5)$$

and

$$\langle n\rangle(t) = \sum_{n,m}[n]|c_{n,m}(t)|^2. \quad (6)$$

For an initial condition with both electrons fully localized at the same site, the spatial symmetry of this initial state and the interaction Hamiltonian provides $\langle m \rangle(t) = \langle n \rangle(t)$. We analyze these quantities and also the mean electronic velocity ($< v_m >= d[\langle m \rangle(t)]/dt$ or $< v_n >= d[\langle n \rangle(t)]/dt$) in order to characterize the electronic transport for this model.

III. RESULTS AND DISCUSSIONS

We start showing and discussing our results for the two-electron propagation within the Morse chain. We stress that our initial condition consists of localizing both electrons at the center of a long self-expanded chain [$c_{n,m}(t = 0) = \delta_{n,N/2}\delta_{m,N/2}$]. In our numerical technique the complete system has about $N = 3500$ sites. However, we first use only a small fraction of these sites. We begin our calculations in a small chain with $N_d = 200$. Whenever the wave function or the atomic vibration arrives at tthe boundary of the initial chain, we expand the size of the initial chain by 20 sites (10 sites on the left and 10 sites on the right of the lattice). By using this trick, the sum of wave probability and atomic vibration value (in modulus) on the boundary of chain can be kept less than 10^{-20}, thus avoiding border effect. We consider the following initial condition for the Morse lattice: $q_n(t = 0) = 0$ and $p_n(t = 0) = +\delta_{n,N/2}$. This procedure injects energy into the Morse lattice and a finite fraction of the energy propagates along the chain in a solitonic mode (due the nonlinear Morse potential) [16,48]. This method, used in several works [12–18,22,45,48], promotes the appearance of a solitonic mode moving along the chain. The direction of *the solitonic modes* movement depends on the sign of initial velocity used to inject vibrational energy into the chain. Considering $p_n(t = 0) = -\delta_{n,N/2}$, the solitonic mode has a reverse trajectory. We remind that only a finite fraction of initial energy is participating in the solitonic-like lattice deformation; the other part evolves along the chain through nonlinear vibrational modes also called radiation [50–54].

A plot of the wave-packet centroid $< n > (t)$ versus time t for $\alpha = 1.75$ and $U = 0,2,4,8,12$ is given in Fig. 1(a). We observe that the electronic position moves to the right side of the chain and that the electronic velocity seems to depend on the level of Coulomb interaction (U). It is time for a brief discussion of the electronic propagation from the angle of electron phonon coupling intensity (α). The case with no electron-lattice coupling ($\alpha = 0$) is observed in the "inset." We see that, in the absence of electron-phonon coupling, mean position remains fixed as time evolves. The electron-lattice coupling promotes electronic displacement due to the presence of solitonic modes within this model. The solitonic behavior can be found by analyzing the lattice deformation in the plot of A_n versus n and t [see Fig. 1(b)]. We emphasize that A_n represents a kind of generalized probability of local deformation. This quantity is obtained as follows: First, we compute the quantity $x_n = (1 - e^{[-q_n + q_{n-1}]})^2$. Second, we normalize x_n to get the generalized probability of local deformation A_n; i.e., $A_n = x_n / \sum_n (x_n)$.

When electron-phonon coupling arises ($\alpha > 0$), the electronic wave function becomes partially trapped by the solitonic modes. Because of the mobility of the solitonic mode, the electron acquires nonzero velocity (they travel with supersonic
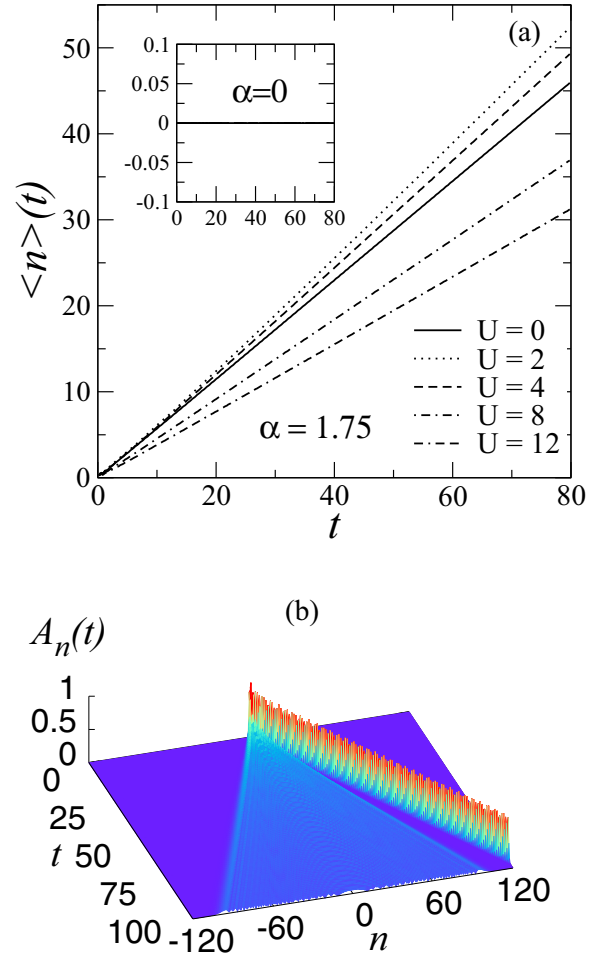
FIG. 1. (a) Wave-packet centroid $< n > (t)$ versus time t for $\alpha = 1.75$ and $U = 0,2,4,8,12$. Inset: $< n > (t)$ versus t for no electron-phonon coupling ($\alpha = 0$) and also $U = 0,2,4,8,12$. $n = 0$ represent the center of chain. The electron-lattice term promotes the coupling between the electronic wave-function and the solitonic modes of the Morse chain. Therefore, a fraction of wave-packet is trapped and therefore the two-electron packet obtain mobility. In the absence of electron-phonon coupling, the two electron state has zero velocity (see inset). (b) Lattice deformation A_n versus n and t for $\alpha = 1.75$ and $U = 0$. It shows the solitonic behavior of the Morse chain. The electronic mean position $< n > (t)$ follow, approximately, the solitonic mode dynamics due to the electron-lattice coupling $\alpha > 0$.

velocity, in general). We stress that the momentum was positive, therefore the solitonic modes propagate to the right side (and as a result, the electron exhibits only positive velocity). By inverting the sign of initial impulse excitation, the solitonic mode (and also the electrons) will travel to the left side of the chain. The authors in Ref. [38] anticipated the trapping of two interacting electrons by the solitonic mode of a Morse lattice using a distinct initial condition. Our interest rests in the investigation of the effect of Coulomb interaction. In order to do this, it was necessary to use an initial two-electron wave packet with at least a large fraction of all bound states components.
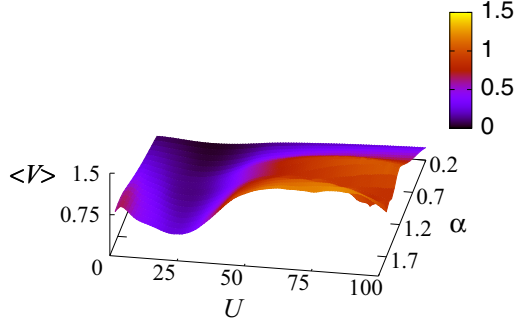
FIG. 2. Electronic velocity $< V >$ versus U and α. We observe that for α in the interval [1.6,2] and $U \approx 3$, there exists a local maximum for the electronic velocity. For $U > 4\tau$ and strong electron-lattice interaction ($\alpha >> 0$) the electron's velocity reaches a plateau.

In Fig. 2, we plot the effective electron velocity $< V >=< v_n >=< v_m >$ versus U and α. This figure was made by solving the model for a wide range of U, α values and the effective velocity for each case was obtained by using a linear fitting of the data for $< n > (t)$ versus t. We kept $\alpha \leqslant 2$. This limit, which was also used in Refs. [16,48], enables us to do all calculations with sufficient numerical accuracy. Analyzing Fig. 2, we notice that for $\alpha \approx 0$, the effective velocity is close to zero and for strong electron-phonon coupling ($\alpha > 1$), the electron in fact exhibits mobility. However, we also found a nontrivial dependence of the electron velocity with the electron-electron coupling. In special, for α within the interval [1.6,2] and $U \approx 3$, we observed a local maximum for the velocity. Also, for strong Coulomb interaction and electron-lattice parameter, the electronic velocity increases until it becomes roughly constant. We emphasize that the velocity is not constant, of course. The velocity for large U and α increases and reaches a rough plateau (see Fig. 2). This behavior needs a more detailed description. Within this two-electron model, we know that, as U is increases, the density of states exhibits a subband of bound states [42]. In the following paragraphs, we will analyze the possible influence of these bound states in this unusual transport.

We compute the one-electron effective wave function defined as $|c_n(t)|^2 = \sum_m |c_{n,m}(t)|^2$. In Figs. 3(a)–3(c), we plot $|c_n(t)|^2$ versus n and t for $\alpha = 1.75$ and $U = 0, 2, 4$. We observe that a finite fraction of the initial wave packet is captured by the nonlinear lattice vibrations and it moves to the right side of the chain. The remnant of the wave packet remains free and spreads for both sides of chain. It is viewed for initial time on Figs. 3(a)–3(c), but we agree that it is hard to be perceived. In Fig. 3(d), we plot $|c_n(t)|^2$ versus n for the same cases showed in Figs. 3(a)–3(c), however, we choose a single moment ($t = 60$ here). In the plot in Fig. 3(d), we observe clearly a finite fraction localized at the right side of the chain and the rest of the wave function spreads free along the chain. The marked peak represents the fraction of wave function that was captured by solitonic mode. The rest of the wave function becomes free to spread within the chain. We will now discuss this behavior in light of the competition between the electron-electron term and the electron-phonon coupling.
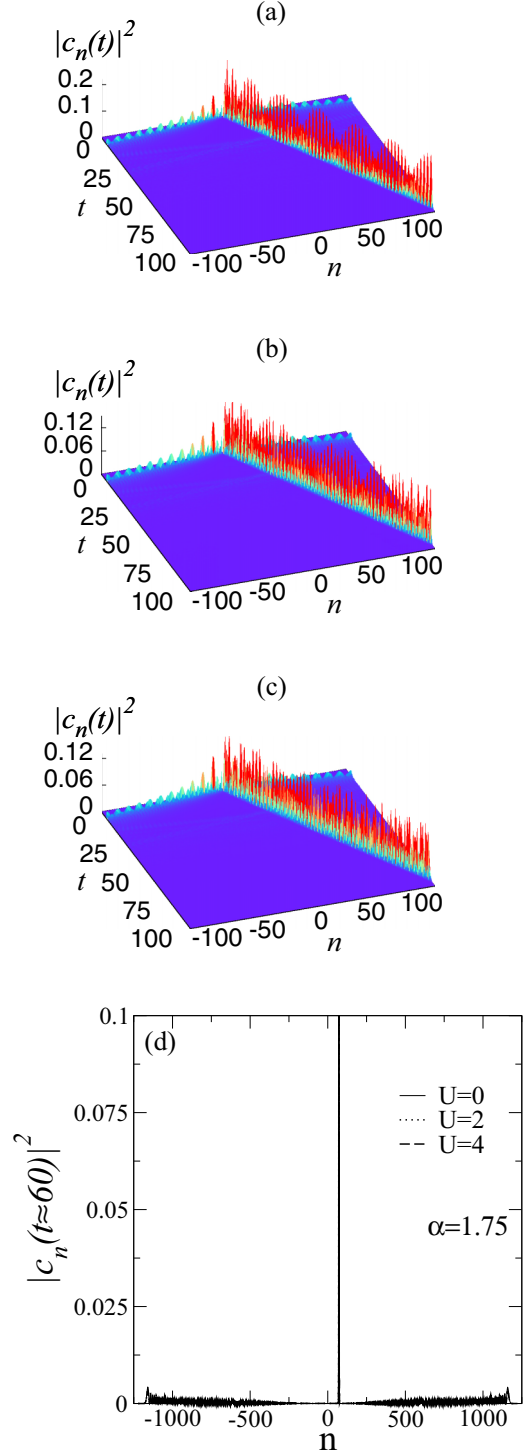
FIG. 3. (a–c) One-electron wave-function ($|c_n(t)|^2 = \sum_m |c_{n,m}(t)|^2$) versus n and t for $\alpha = 1.75$ and $U = $ (a) 0, (b) 2, and (c) 4. (d) $|c_n(t)|^2$ versus n for the same cases in (a–c), for the moment $t \approx 60$. We observe a finite fraction of the initial wave packet captured by the solitonic mode and moved together with it. The remainder of the wave function spreads along the chain.

The initial two-electron wave packet is a superposition of all two-electron eigenstates. Due to the shape of the initial two-electron wave packet (i.e., a δ function), the eigenstates that have an initial small distance between both electrons play a major role in the long-time evolution. Within the

two-electron subspace that we are dealing with, there is a collection of eigenstates in which the electron-electron distance is zero (or almost zero). These states are called bound states [42,55]. We will *revisit* now some concepts about these states and its dependence with the electron-electron interaction intensity U.

For $U = 0$, the density of states for the two-electron Hamiltonian is exactly the same as that obtained for the one-electron 2D Anderson Model. For $U > 0$, a new subband of two-electron bound states appears. It was already proved that the subband of bound states can be found within the interval $[U, \sqrt{U + 16Z^2}]$, where Z represents the effective hopping [42,55]. Here, in our model, the hopping energy is time-dependent quantity ($T_{n,n+1} = -\tau \exp[-\alpha(q_{n+1} - q_n)]$). In order to study the two-electron band structure of the present model, we consider the quantity Z as the mean value of our time-dependent hopping (i.e., $Z \approx < T_{n,n+1} > \approx \tau = 10$). Therefore, the two-electron free band covers the interval $[-4\tau, 4\tau]$ [42,55] and $U < 4\tau$ represents the "weak" Coulomb interaction limit. We used the word "weak" so as to classify the regime in which that free band and bound state band remains merged. In the strong limit ($U > 4\tau$), the free band and the bound state band are decoupled. Moreover, the width of the bound state subband decreases [42,55]. Therefore, the number of bound states within the initial wave packet decreases for $U > 4\tau$.

The dependence of the effective electronic velocity with the value of U is quite related with the appearance of bound states and its competition with the electron-lattice coupling. In order to provide a better understanding of the relation between the existence of bound states and the electron-soliton dynamics, we investigated the two-electron wave-function framework. We plot $|c_{n,m}(t \approx 50)|^2$ versus n and m for $\alpha = 1.75$ and $U = 0, 1, 2, 3$ [Figs. 4(a)–4(d)] and $U = 60, 80, 100$ [Figs. 5(a)–5(c)]. In Fig. 4, we observe the effect of bound states as well as the one-electron free component. For $U = 0$ a finite fraction of the wave function remains trapped close to the center of plane $n \times m$. This fraction represents the portion of the wave function that was captured by the solitonic mode. Furthermore, there are two branches of the wave function that travel free along the n and m directions. These branches represent the free electron components. As the electron-electron term is increased ($U = 1, 2, 3$), we got previous behavior combined to a finite fraction of the wave function, which remains "trapped" along the diagonal of the plane $n \times m$. This diagonal wave represent the states with $n \approx m$, i.e., the bound states. Therefore, in spite of the electron-soliton coupling being sufficient to capture a finite fraction of the two-electron wave function, a free component and also another component deriving from the bound states are still present in the dynamics. Thus, as the Coulomb term is increased, a competition between the electron-lattice term and the dynamics of the free and bounded components occurs. Within the weak Coulomb interaction $U << 4\tau$, both the free and bound subband are "merged." It means electron-soliton coupling can capture both components. When Coulomb interaction is at strong limit $U > 4\tau$ (see Fig. 5), results change drastically. We observe a large fraction of the wave function on the diagonal of the plane $n \times m$, while the free one becomes sufficiently small.
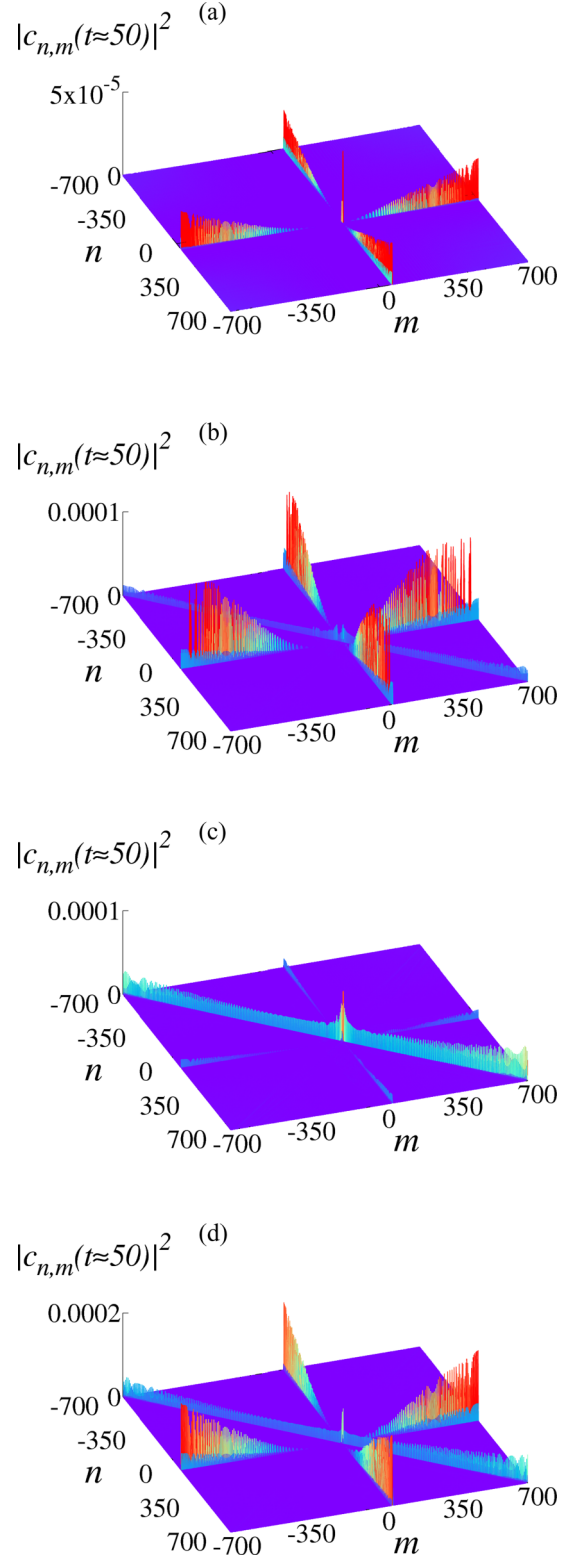
FIG. 4. Two-electron wave-function for $t \approx 50$ ($|c_{n,m}(t \approx 50)|^2$) versus n and m for $U =$ (a) 0, (b) 1, (c) 2, and (d) 3. For $U = 0$ a finite fraction of the wave function remains captured by the solitonic mode close to the center of plane $n \times m$. Moreover, there are two branches of the wave function that travel free along n and m direction. For $U = 1, 2, 3$, we also observed in addition to the previous situation, that a finite fraction of the wave-function remains "trapped" along the diagonal of the plane $n \times m$, i.e., bound states.
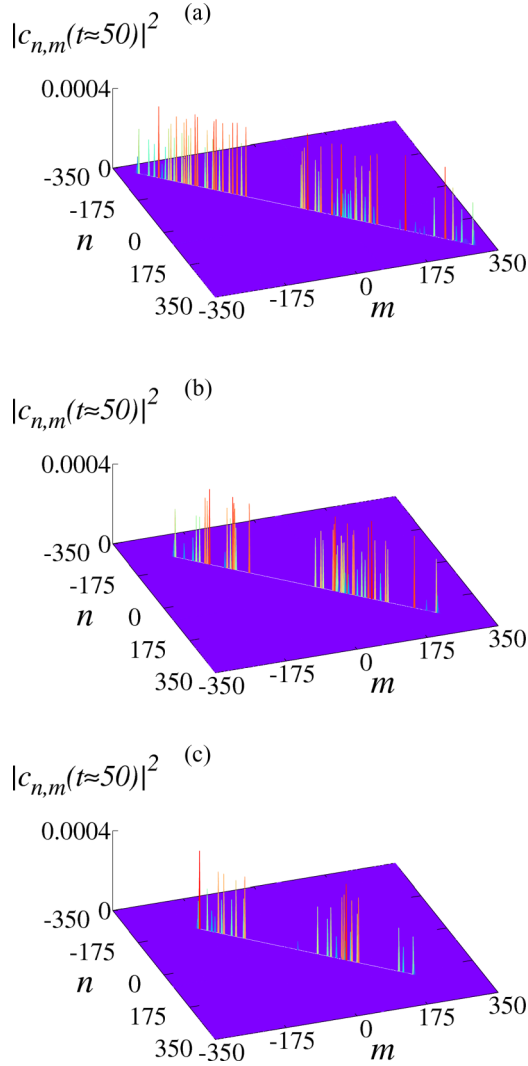
FIG. 5. The same kind of plot as in Fig. 4, i.e., $|c_{n,m}(t \approx 50)|^2$ versus n and m for $U =$ (a) 60, (b) 80, and (c) 100. For strong U the bound states become dominant and the solitonic mode capture a finite fraction of those states, thus promoting dynamics along the line $n \approx m$. This behavior also promotes increased velocity in the limit of $U > 4\tau$ and strong electron-lattice interaction ($\alpha \gg 0$).

Let's discuss qualitatively these results for strong U. We stress, at first, that for $U > 4\tau$ the subbands related with the free and the bound eigenstates are not merged, so they are decoupled and become more apart as U increases. Second, the initial condition type we have chosen (i.e., both electrons fully initially localized) favors a minor free state subband contribution in comparison to bound ones. Accordingly, for strong U the initial wave packet is roughly a superposition of many bound states. Due to the type of localized solitonic mode we have in the Morse chain, it is easier to capture the bound states component of a two electron wave packet. A portion of initial wave packet related to the bound eigenstates are trapped by the solitonic mode and move along the chain. In short, for weak U, the solitonic mode captures both free and bounded components then, the competition between these distinct dynamics decreases the velocity. On the other hand, for strong U, the bound states dominate and the electrons

remain together. Therefore, this "coupled pair" is captured by the solitonic mode more easily. This feature is behind the increasing of velocity within the limit of strong U and α.

Before concluding our work, we will make a brief explanation of the kind of two-electron initial wave packet we have used. The dependence of the electronic velocity with the Coulomb interaction and electron-lattice term is broadly associated with the bound states inside the initial two-electron wave packet. We stress that the initial fully localized two-electron wave packet we have used exhibit a huge fraction of two-electron bound states [42]. Therefore, Coulomb interaction plays a relevant role controlling electron's velocity. An interesting question that arises in this problem is to understand what would happen if we initially put the electrons in different positions. With this kind of initial condition, the number of bound states in the initial wave packet decreases a lot. In addition, we also change the position in which the vibrational energy is injected into the lattice. Considering $c_{n,m}(t = 0) = \delta_{n,n_0}\delta_{m,m_0}$ with $n_0 = N/2 - 30$, $m_0 = N/2 + 30$ and impulse excitation as $q_n(t = 0) = 0$ and $p_n(t = 0) = +\delta_{n,N/2-50}$, we solve the coupled set of quantum/classical equations. A summary of results obtained for $U = 0, 8, 16$ and $\alpha = 0$ and 1.75 is shown in Figs. 6(a)–6(c). We remind that the mean position was shifted such that $< n > (t) =< m > (t) = 0$ is the center of chain. For $\alpha = 0$ and $U = 0$ [see Fig. 6(a)], we observe that mean position of each electron is constant, therefore the velocity is zero. In the absence of electron-lattice term ($\alpha = 0$), both electrons do not interact with the nonlinear vibrational modes. Consequently, the solitonic mode that appear in the Morse lattice does not capture the electrons and they remain with no mobility. As the Coulomb interaction is increased, even in the absence of electron-lattice interaction, both electrons trend to move apart. It is an outcome of the type of initial condition and the Coulomb term. As the initial state does not contain many bound-states, electrons avoid occupying the same position when U increases (electron-electron repulsion).

In Figs. 6(b) and 6(c), we show some calculations for the case with electron-lattice interaction ($\alpha = 1.75$). We stress again that the impulse excitation it was injected at position $N/2 - 50$. It is noticeable, in Fig. 6(b), that vibrational energy spreads within the chain and promotes also rise of a solitonic vibrational mode that propagates from the bottom ($n < 0$) to the top of chain ($n > 0$). This nonlinear propagation of energy captures a finite fraction of the wave function of each electron and then pushes both electrons to the same direction. We can see this interesting phenomenon by analyzing the Fig. 6(c). The mean position of each electron evolves to the top of chain ($n > 0$), however, the velocity of each electron is different. We observed that, for $U = 0, 8$, the electron that was initially localized closer to the vibrational energy input propagates with largest velocity. The main explanation for this difference in the velocity is the distance between the electron and the solitonic mode at the beginning of dynamics: The larger the distance, the more difficult for solitonic mode capture a finite fraction of the electronic wave-packet. Moreover, we also have the effect of Coulomb interaction repelling both electrons. We observe this repulsion effect by analyzing the meeting time for the electronic centroids. We observe that as U is increased the meeting time also increases. This is a clear signature of
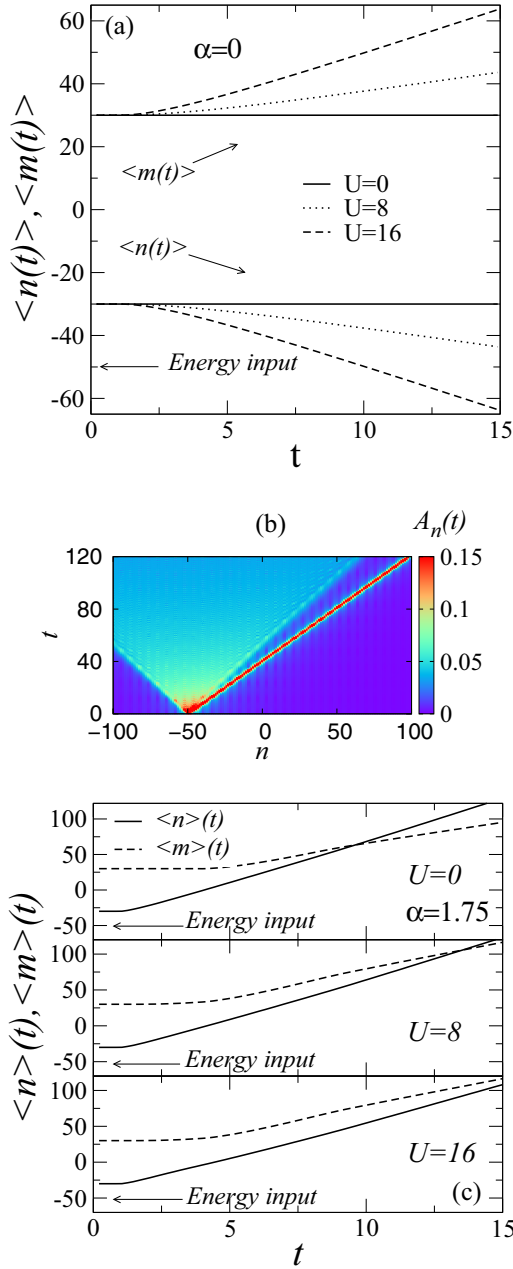
FIG. 6. (a) Mean position of each electron for $U = 0, 8, 16$ and $\alpha = 0$. (b) Lattice deformation A_n versus t and n for $U = 16$ and $\alpha = 1.75$. (c) Mean position of each electron for $U = 0, 8, 16$ and $\alpha = 1.75$. Calculations were done considering $c_{n,m}(t = 0) = \delta_{n,n_0}\delta_{m,m_0}$ with $n_0 = N/2 - 30$ and $m_0 = N/2 + 30$ and $q_n(t = 0) = 0$ and $p_n(t = 0) = +\delta_{n,N/2-50}$.

FIG. 7. (a–d) One-electron wave function $|c_n(t)|^2$ and $|c_m(t)|^2$ versus time t and the site index (n for one electron and m for the other one). Calculations were done for the same type of initial condition as in Fig. 6 with (a, b) $U = 0$ and (c, d) $U = 16$.

the effective repulsion between both electrons for $U > 0$ and for this type of initial condition. In Figs. 7(a)–7(d) we plot the one-electron wave function $|c_n(t)|^2$ and $|c_m(t)|^2$ versus time t and site index (n for one electron and m for the other one). We used a 2D color mapping scheme to improve visualization. Calculations were done for $U = 0$ and 16. In agreement with our previous calculations of the centroid trajectories, the most part of the one-electron wave-function moves to the positive side of chain ($n > 0$) due to the coupling with nonlinear vibrational modes. Compare Figs. 7(a)–7(d) with

Fig. 6(b). We observe that the two electron wave-packet is "pushed" to the right side due to the presence of solitonic mode. In Figs. 8(a)–8(f), we show a brief summary of our results for the following initial conditions: the two-electron wave-packet is defined as $c_{n,m}(t = 0) = \delta_{n,n_0}\delta_{m,m_0}$ with $n_0 = N/2 - 30$, $m_0 = N/2 + 30$ and impulse excitation as $q_n(t = 0) = 0$, $p_n(t = 0) = +\delta_{n,N/2-30}$ and $p_n(t = 0) = -\delta_{n,N/2+30}$. Therefore, for $t = 0$, we have one electron located at site n_0 and the other electron located at site m_0. We name these electrons as electron "n" and electron "m." Also, we have two initial impulse excitations located at the same site of each electron with distinct velocity sign. That produces solitonic modes
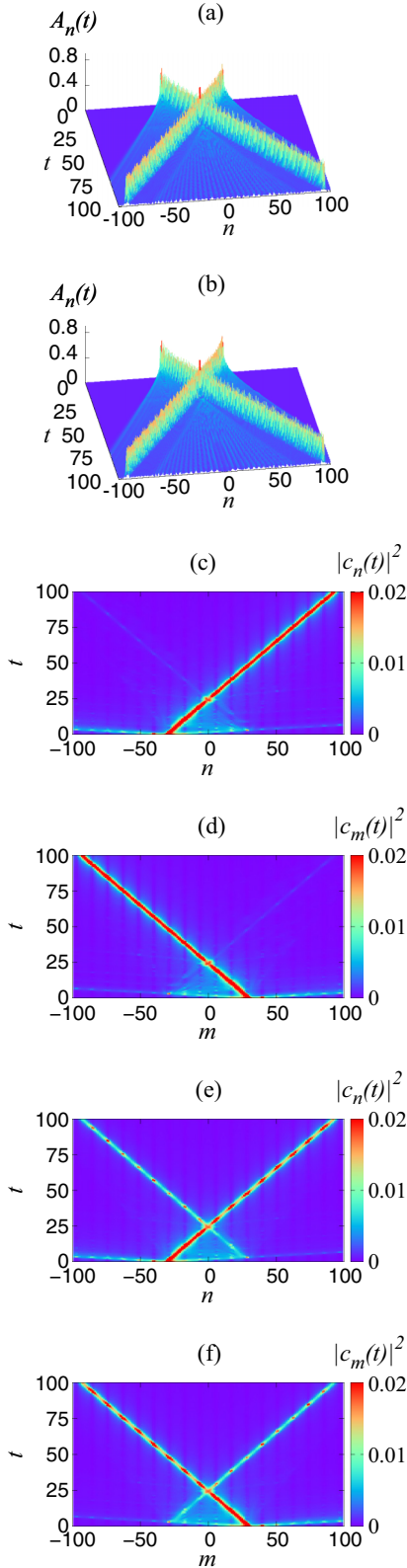
FIG. 8. (a, b) Lattice deformation A_n versus n and t for $\alpha = 1.75$ and $U = $ (a) 0 and (b) 16. (c, d) One-electron wave function $|c_n(t)|^2$ and $|c_m(t)|^2$ versus time t and the site index (n for one electron and m for the other one) for $U = 0$. (e, f) the same as in (c, d) for $U = 16$. The initial conditions are: $c_{n,m}(t = 0) = \delta_{n,n_0}\delta_{m,m_0}$ with $n_0 = N/2 - 30$, $m_0 = N/2 + 30$ and impulse excitation as $q_n(t = 0) = 0$, $p_n(t = 0) = +\delta_{n,N/2-30}$ and $p_n(t = 0) = -\delta_{n,N/2+30}$.

which travel in opposite directions. In Figs. 8(a) and 8(b), we clearly observe the presence of two solitonic modes and also a small amount of energy that spreads along the chain (also called radiation, as noticed in [22,50–54]). These solitonic modes travel in opposite directions and then collide in a time between {20,30} units. The phenomenon of solitons' collision is well known in the literature. In general, both solitonic modes collide without any change in his directions or intensity, exactly as it is shown in the figure 8(a,b). We also observed that the main profile of Figs. 8(a) and 8(b) does not exhibit any dependence with the Coulomb interaction. In Figs. 8(c)–8(f), we see one-electron wave function $|c_n(t)|^2$ and $|c_m(t)|^2$ versus time t and site index (n for one electron and m for the other one). For $U = 0$ the main result is quite similar to the one observed in Ref. [17] for a single particle: the solitonic mode captures a fraction of the wave-function and pushes it along the chain [see Figs. 8(c) and 8(d)]. For $U = 16$, we observe an interesting phenomenon quite related to the Coulomb interaction and the electron-phonon coupling. For a better understanding, lets discuss it in more detail: First, we need to remind that two solitonic modes were generated at different positions n_0 and m_0. We call these solitonic modes as the solitonic mode "n" and solitonic mode "m," respectively. These solitonic modes capture each one a fraction of the electronic wave function which was initially localized at sites n_0 and m_0. Moreover, besides the fractions of wave functions that were captured by the solitonic modes "n" and "m," there is still a fraction of the two electron wave-function that remains free to move along the chain (we see it in these figures and also in Figs. 1 and 2). The soliton-electron pair that starts at site $n_0 = N/2 - 30$ (called "electron-soliton n") meets the "electron-soliton m" and also the free part of the wave-function of the electron "m." Due to de presence of Coulomb interaction, the fraction of bound states that exists within this kind of initial condition can be easily captured by the solitonic mode. Therefore, a finite fraction of the electron "n" remains trapped by the solitonic mode "n" and a small fraction of the bounded states is trapped by the other solitonic mode "m"). The same phenomenon occurs for the electron "m." Therefore, the presence of Coulomb interaction and the kind of initial condition plays relevant role in the electron-phonon dynamics. In Figs. 9(a) and 9(b), we plot the lattice deformation (A_n) and the one-electron wave-function ($|c_n|^2$ and $|c_m|^2$) versus n (and m) for the same experiments as in Figs. 8(a)–8(f). We choose two instants: $t \approx 20$ and $t \approx 40$, i.e., before and after the collision of both solitonic modes [see Fig. 8(a)]. We observe that the lattice deformations exhibit a mobile and stable solitonic-like profile and a small amount of energy that spreads along the chain (in good agreement with previous works [17,22,45,50–54]). We also observe the electron-phonon dynamics in detail: the stable solitonic-like deformation captures a finite fraction of the wave packet and the other part evolves in time interacting with the radiation process.

IV. SUMMARY AND CONCLUSIONS

In this paper, we considered the problem of two interacting electrons moving under effect of electron-phonon interaction. Therefore, by using our formalism, the competition between
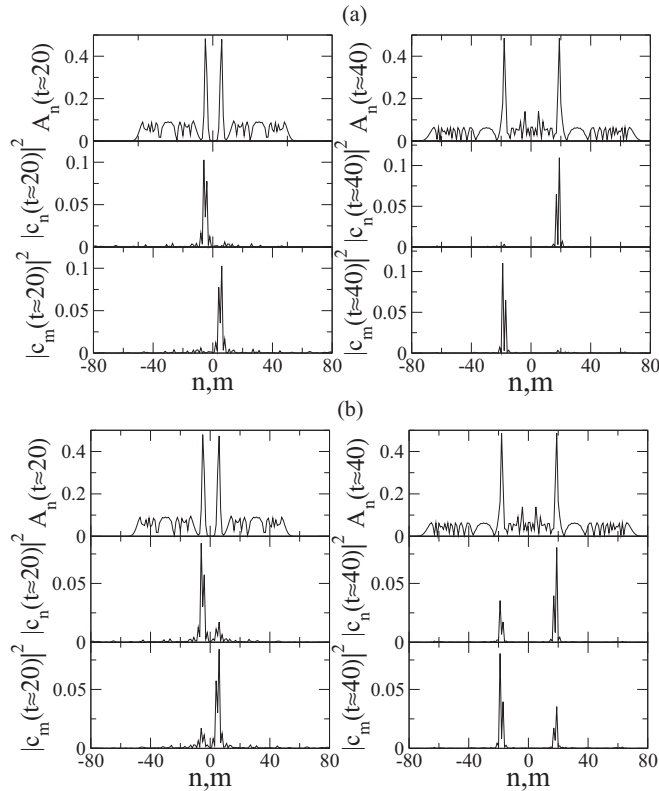
FIG. 9. Lattice deformation (A_n) and one-electron wave function ($|c_n|^2$ and $|c_m|^2$) versus n (and m) for the same experiments as in Figs. 8(a–f) with (a) $U = 0$ and (b) $U = 16$. We choose two time instants: $t \approx 20$ and $t \approx 40$, i.e., before and after the collision of solitonic modes [see Fig. 8(a)].

the electron-lattice coupling and electron-electron interaction was investigated. We considered the singlet subspace of a

standard two-electron Hamiltonian and we used a nonlinear Morse lattice as a substrate. As initial condition, both electrons were placed at half-chain position and an impulse excitation started at the same locus in order to create a solitonic mode. Using numerical methods, we solved quantum and classical equations for this problem and we tracked the electronic dynamics. Our results suggest the possibility of both electrons being trapped by the solitonic mode and, consequently, the rise of effective velocity of collective excitation. We also noticed that the electron velocity depends on the Coulomb interaction as well as on the intensity of the electron-lattice interaction. Analyzing the wave-function topology for a long time, we found some new and interesting information about the nature of two-electron-soliton coupling: the presence of bound states plays relevant role within the dynamics. The existence of bound states in the initial condition and their relation to the degree of the Coulomb interaction was used to explain qualitatively the electronic velocity in our model. We also discussed briefly the electronic dynamics by considering the electrons initially separated. Our results show that the electronic velocity exhibits an interesting and new kind of dependence with the Coulomb interaction. In particular, we demonstrated that in the case of distant electrons (initial condition), it is possible to find clear signature of electron-electron repulsion in time-dependent calculations. The electron-electron repulsion is a direct consequence of the Coulomb interaction and of the type of initial two-electron wave-packet.

[1] P. K Datta and K. Kundu, Phys. Rev. B **53**, 14929 (1996).

[2] G. Kopidakis, S. Komineas, S. Flach, and S. Aubry, Phys. Rev. Lett. **100**, 084103 (2008).

[3] F. A. B. F. de Moura, Iram Gléria, I. F. dos Santos, and M. L. Lyra, Phys Rev. Lett. **103**, 096401 (2009).

[4] Ch. Skokos, D. O. Krimer, S. Komineas, and S. Flach, Phys. Rev. E **79**, 056211 (2009); **89**, 029907(E) (2014).

[5] Z. Pan, S. Xiong, and C. Gong, Phys. Rev. E **56**, 4744 (1997).

[6] S. Tietsche and A. Pikovsky, Europhys. Lett. **84**, 10006 (2008).

[7] A. S. Davydov, *Solitons in Molecular Systems*, 2nd ed. (Reidel, Dordrecht, 1991).

[8] A. C. Scott, Phys. Rep. **217**, 1 (1992).

[9] A. S. Davydov, Phys. Scr. **20**, 387 (1979).

[10] A. S. Davydov, J. Theor. Biol. **66**, 379 (1977).

[11] A. S. Davydov, *Biology and Quantum Mechanics* (Pergamon, New York, 1982).

[12] B. J. Alder, K. J. Runge, and R. T. Scalettar, Phys. Rev. Lett. **79**, 3022 (1997).

[13] L. S. Brizhik and A. A. Eremko, Physica D **81**, 295 (1995).

[14] O. G. C. Ross, L. Cruzeiro, M. G. Velarde, and W. Ebeling, Eur. Phys. J. B **80**, 545 (2011).

[15] M. G. Velarde and C. Neissner, Int. J. Bifurcat. Chaos **18**, 885 (2008).

[16] D. Hennig, A. Chetverikov, M. G. Velarde, and W. Ebeling, Phys. Rev. E **76**, 046602 (2007).

[17] V. A. Makarov, M. G. Velarde, A. P. Chetverikov, and W. Ebeling, Phys. Rev. E **73**, 066626 (2006).

[18] D. Hennig, C. Neißner, M. G. Velarde, and W. Ebeling, Phys. Rev. B **73**, 024306 (2006).

[19] M. G. Velarde, W. Ebeling, and A. P. Chetverikov, Int. J. Bifurcat. Chaos **21**, 1595 (2011).

[20] A. P. Chetverikov, W. Ebeling, and M. G. Velarde, Eur. Phys. J. B **80**, 137 (2011).

[21] M. G. Velarde, W. Ebeling, and A. P. Chetverikov, Internat. J. Bifurcat. Chaos **15**, 245 (2005).

[22] M. G. Velarde, J. Comput. Appl. Math. **233**, 1432 (2010).

[23] A. P. Chetverikov, W. Ebeling, and M. G. Velarde, Eur. Phys. J. B **85**, 291 (2012).

[24] W. Ebeling, A. P. Chetverikov, G. Röpke, and M. G. Velarde, Contrib. Plasma Phys. **53**, 736 (2013).

[25] A. P. Chetverikov, W. Ebeling, and M. G. Velarde, Eur. Phys. J. Special topics **222**, 2531 (2013).

[26] M. G. Velarde, A. P. Chetverikov, W. Ebeling, E. G. Wilson, and K. J. Donovan, Europhys. Lett. **106**, 27004 (2014).

[27] A. P. Chetverikov, W. Ebeling, and M. G. Velarde, Eur. Phys. J. B **89**, 196 (2016).

[28] M. R. Astley, M. Kataoka, C. J. B. Ford, C. H. W. Barnes, D. Anderson, G. A. C. Jones, I. Farrer, D. A. Ritchie, and M. Pepper, Phys. Rev. Lett. **99**, 156802 (2007).

[29] S. Hermelin, S. Takada, M. Yamamoto, S. Tarucha, A. D. Wieck, L. Saminadayar, C. Bäuerle, and T. Meunier, Nature **477**, 435 (2011).

[30] R. P. G. McNeil, M. Kataoka, C. J. B. Ford, C. H. W. Barnes, D. Anderson, G. A. C. Jones, I. Farrer, and D. A. Ritchie, Nature **477**, 439 (2011).

[31] M. Kataoka, M. R. Astley, A. L. Thorn, D. K. L. Oi, C. H. W. Barnes, C. J. B. Ford, D. Anderson, G. A. C. Jones, I. Farrer, D. A. Ritchie, and M. Pepper, Phys. Rev. Lett. **102**, 156801 (2009).

[32] C. H. W. Barnes, J. M. Shilton, and A. M. Robinson, Phys. Rev. B **62**, 8410 (2000).

[33] H. Sanada, T. Sogawa, H. Gotoh, K. Onomitsu, M. Kohda, J. Nitta, and P. V. Santos, Phys. Rev. Lett. **106**, 216602 (2011).

[34] M. R. Astleya, M. Kataokaa, C. J. B. Forda, C. H. W. Barnesa, D. Andersona, G. A. C. Jonesa, I. Farrera, D. A. Ritchiea, and M. Peppera, Physica E **40**, 1136 (2008).

[35] S. Völk, F. J. R. Schülein, F. Knall, D. Reuter, A. D. Wieck, T. A. Truong, H. Kim, P. M. Petroff, A. Wixforth, and H. J. Krenner, Nano Lett. **10**, 3399 (2010).

[36] F. J. R. Schülein, K. Müller, M. Bichler, G. Koblmüller, J. J. Finley, A. Wixforth, and H. J. Krenner, Phys. Rev. B **88**, 085307 (2013).

[37] E. Z. Kuchinskii, I. A. Nekrasov, and M. V. Sadovskii, Phys. Rev. B **80**, 115124 (2009).

[38] D. Hennig, M. G. Velarde, W. Ebeling, and A. Chetverikov, Phys. Rev. E **78**, 066606 (2008).

[39] Y.-F. Yang and K. Held, Phys. Rev. B **76**, 212401 (2007).

[40] L. Cruzeiro, J. C. Eilbeck, J. L. Marín, and F. M. Russell, Eur. Phys. J. B **42**, 95 (2004).

[41] W. S. Dias, M. L. Lyra, and F. A. B. F. de Moura, Eur. Phys. J. B **85**, 7 (2012).

[42] W. S. Dias, E. M. Nascimento, M. L. Lyra, and F. A. B. F. de Moura, Phys. Rev. B **76**, 155124 (2007).

[43] J. Hubbard, Proc. R. Soc. London A **276**, 238 (1963).

[44] W. P. Su, J. R. Schrieffer, and A. J. Heeger, Phys. Rev. Lett. **42**, 1698 (1979).

[45] M. O. Sales and F. A. B. F. de Moura, J. Phys.: Condens. Matter **26**, 415401 (2014).

[46] F. A. B. F. de Moura, Int. J. M. Phys. C **22**, 63 (2011).

[47] E. Hairer, S. P. Norsett, and G. Wanner, *Solving Ordinary Dierential Equations I: Nonstiff Problems*, Springer Series in Computational Mathematics, 2nd revised ed. (Springer-Verlag, New York, NY, 1993); W. H. Press, B. P. Flannery, S. A. Teukolsky, and W. T. Wetterling, *Numerical Recipes: The Art of Scientific Computing*, 3rd ed. (Cambridge University Press, New York, 2007).

[48] A. R. Neto and F. A. B. F. de. Moura, Commun Nonlinear Sci. Numer. Simulat. **40**, 6 (2016).

[49] A. R. Neto, M. O. Sales, and F. A. B. F. de Moura, Solid State Commun. **229**, 22 (2016).

[50] N. F. Smyth and A. L. Worthy, Phys. Rev. E **60**, 2330 (1999).

[51] Y. S. Kivshar, J. Phys. A: Math. Gen. **22**, 337 (1989).

[52] W. L. Kath and N. F. Smyth, Phys. Rev. E **51**, 661 (1995).

[53] C. A. A. dos Santos, T. F. Assunção, M. L. Lyra, and F. A. B. F. de Moura, Int. J. M. Phys. C **23**, 1240009 (2012).

[54] G. S. Zavt, M. Wagner, and A. Lütze, Phys. Rev. E **47**, 4108 (1993).

[55] F. Claro, J. F. Weisz, and S. Curilef, Phys. Rev. B **67**, 193101 (2003).